Polarimetric Image Segmentation via Maximum-Likelihood Approximation and Efficient Multiphase Level-Sets

Ismail Ben Ayed, *Student Member, IEEE*, Amar Mitiche, *Member, IEEE*, and
Ziad Belhadj, *Member, IEEE*

Abstract—This study investigates a level set method for complex polarimetric image segmentation. It consists of minimizing a functional containing an original observation term derived from maximum-likelihood approximation and a complex Wishart/Gaussian image representation and a classical boundary length prior. The minimization is carried out efficiently by a new multiphase method which embeds a simple partition constraint directly in curve evolution to guarantee a partition of the image domain from an arbitrary initial partition. Results are shown on both synthetic and real images. Quantitative performance evaluation and comparisons are also given.

Index Terms—Polarimetric images, complex Wishart distribution, complex Gaussian distribution, level set active contour segmentation, maximum-likelihood approximation.

✦

1 INTRODUCTION

THE variational, active contour/level set formalism leads to effective segmentation algorithms [1], [2], [3], [4], [5], [6], [7]. This formalism has been developed for and mainly applied to intensity data acquired by conventional cameras [8],[9], [1] [2], [3], [4], [5]. For such images, the piecewise constant and Gaussian models are often sufficient and almost all investigations have used them. However, there are other important and quite different images, polarimetric, for instance, for which these models are inadequate, as studies have shown [10], [7]. The study in [10] shows the influence of the noise model on level set segmentation, demonstrating the necessity to use an appropriate model. In [7], we investigated a segmentation functional with a Gamma distribution observation model for Synthetic Aperture Radar (SAR) images. Such radar images are quite poorly modeled by piecewise constant and Gaussian models.

Following on from our initial effort in [7] to develop efficient level set segmentation algorithms for important classes of images, the present study investigates polarimetric image segmentation. Segmentation of polarimetric images plays an essential role in medical imaging [11] and remote sensing [12]. A polarimetric image sensor applies a wave scattering mechanism and different transmission/reception wave polarizations to acquire a signal which consists, at each pixel, of a 3×3 complex matrix containing both amplitude and phase information. Segmentation of such images is significantly complicated by the complexity of the data, the occurrence of multiplicative random speckle noise due to signal interference and, highly overlapped region distributions. The presence of speckle in polarimetric images has been addressed in several ways, notably edge detection filters [13], clustering [14], region merging [12], and Markov random field modeling [15]. Local operations, preprocessing, post-processing, and several threshold parameters are generally involved, resulting in methods which lack the flexibility and robustness of variational level set methods. The purpose of this study is to investigate a variational method for multiphase segmentation of polarimetric images, both mono-look and multilook, using a complex Wishart/Gaussian observation model [14], [13], [16] and active contours via level-sets. The objective functional contains an original data term, derived from a probabilistic interpretation, which measures the conformity of the data to a complex Wishart/Gaussian distribution in each segmentation region and the classic boundary length prior for smooth segmentation boundaries. We also investigate an efficient minimization scheme which results in an unambiguous multiphase segmentation, i.e., a partition of the image domain. This scheme embeds a simple partition constraint directly in the region competition: if a point leaves a region, it goes to a single other region. We will show that the resulting evolution of curves is robust to initialization and is more efficient than with other schemes which define partitions by mapping regions to the interior of closed curves and their intersections [3], [5] or add a term to the objective functional so as to draw the segmentation toward a partition [17], [1]. The complexity of the methods in [3], [5] increases significantly with the number of regions as will be discussed in Section 2.6. The methods in [17], [1] do not guarantee a partition. Curve evolution will likely gives an ambiguous segmentation if the partition constraint is not sufficiently enforced and if it is strongly enforced the curves will evolve more as a result of the partition constraint than of image statistics.

We describe experiments which verify the method and its implementation. We include a quantitative evaluation

---

● *I. Ben Ayed and A. Mitiche are with the Institut National de la Recherche Scientifique, INRS-EMT 800, de La Gauchetière Ouest, Montréal, QC, H5A 1K6, Canada. E-mail: {benayedi, mitiche}@emt.inrs.ca.*
● *Z. Belhadj is with École Supérieure des Communications de Tunis (SUP'COM), Cité Technologique des Communications de Tunis, 2083, Tunisia. E-mail: ziad.belhadj@supcom.rnu.tn.*

and comparisons. We also provide experiments to verify the robustness of the method to initial conditions.

2   FORMULATION

Let $\Omega \subset \mathbb{R}$ be the domain of a polarimetric image. The image consists, at each pixel $\mathbf{x} \in \Omega$, of a 3×3 complex Hermitian positive definite matrix $D(\mathbf{x})$. Let $P(D/\mathbf{R})$ be the assumed distribution of D in a region $\mathbf{R} \subset \Omega$. A segmentation is a partition $\{\mathbf{R}_k\}_{k=1}^N$ of the image domain. Segmentation into N regions as Bayesian estimation consists in determining a partition $\{\hat{\mathbf{R}}_k\}_{k=1}^N$ of maximum a posteriori probability over all N-region partitions:

$$
\begin{aligned}
\{\hat{\mathbf{R}}_k\}_{k=1}^N &= \arg \max_{\mathbf{R}_k \subset \Omega} P\Big(\{\mathbf{R}_k\}_{k=1}^N / D\Big) \\
&= \arg \max_{\mathbf{R}_k \subset \Omega} P\Big(D/\{\mathbf{R}_k\}_{k=1}^N\Big) P\Big(\{\mathbf{R}_k\}_{k=1}^N\Big).
\end{aligned}
\tag{1}
$$

Assuming conditional independence between $D(\mathbf{x})$ and $D(\mathbf{y})$ for $\mathbf{x} \neq \mathbf{y}$, and taking the negative of the logarithm in (1), this Bayesian estimation is converted to the following minimization problem:

$$
\{\hat{\mathbf{R}}_k\}_{k=1}^N = \arg \min_{\mathbf{R}_k \subset \Omega} \mathbf{E}[\{\mathbf{R}_k\}_{k=1}^N],
\tag{2}
$$

where the energy $\mathbf{E}[\{\mathbf{R}_k\}_{k=1}^N]$ is defined by:

$$
\begin{aligned}
\mathbf{E}\Big[\{\mathbf{R}_k\}_{k=1}^N\Big] = &\sum_{k=1}^N \int_{\mathbf{x} \in \mathbf{R}_k} -\log P(D(\mathbf{x})/\mathbf{R}_k) d\mathbf{x} \\
&- \log P\Big(\{\mathbf{R}_k\}_{k=1}^N\Big).
\end{aligned}
\tag{3}
$$

2.1   Segmentation via Active Curves

Consider a family of closed parametric curves $\vec{\gamma}_k : [0,1] \rightarrow \Omega, k = 1, \ldots, N-1$, their interior $\mathbf{R}_{\vec{\gamma}_k}$ defining the regions $\mathbf{R}_k|_{k=1,\ldots,N-1}$. Let region $\mathbf{R}_N$ be the intersection of the exteriors of all curves: $\mathbf{R}_N = \bigcap_{k=1}^{N-1} \mathbf{R}_k^c$. The maximum a posteriori partition estimation is converted to a maximum a posteriori estimation of plane curves:

$$
\{\hat{\vec{\gamma}}_k\}_{k=1}^{N-1} = \arg \min_{\vec{\gamma}_k : [0,1] \rightarrow \Omega} \mathbf{E}\Big[\{\vec{\gamma}_k\}_{k=1}^{N-1}\Big],
\tag{4}
$$

where:

$$
\begin{aligned}
&\mathbf{E}\Big[\{\vec{\gamma}_k\}_{k=1}^{N-1}\Big] = \\
&\underbrace{\sum_{k=1}^N \int_{\mathbf{x} \in \mathbf{R}_k} -\log P(D(\mathbf{x})/\mathbf{R}_k) d\mathbf{x}}_{\mathcal{L}} \underbrace{- \log P\Big(\{\vec{\gamma}_k\}_{k=1}^{N-1}\Big)}_{\mathcal{P}}.
\end{aligned}
\tag{5}
$$

For smooth segmentation boundaries, we take the prior term $\mathcal{P}$ as the classic boundary length term [8]:

$$
\mathcal{P} = -\log P\Big(\{\vec{\gamma}_k\}_{k=1}^{N-1}\Big) = \lambda \sum_{k=1}^{N-1} \oint_{\vec{\gamma}_k} ds.
\tag{6}
$$

The likelihood term $\mathcal{L}$ is specified by an observation model, as will be described subsequently.

2.2   The Complex Wishart Observation Model

In the case of multilook polarimetric images, $D(\mathbf{x})$ is assumed to be a random complex matrix following the Wishart distribution [12], [13], [14]:

$$
P(D(\mathbf{x})|\mathbf{R}) = \frac{(\det D(\mathbf{x}))^{L-n} exp\{-L.tr(\Sigma_{\mathbf{R}}^{-1} D(\mathbf{x}))\}}{K(L,n)(\det \Sigma_{\mathbf{R}})^L},
\tag{7}
$$

where $\Sigma_{\mathbf{R}}$ is the covariance matrix of region $\mathbf{R}$ and $K(L,n) = \pi^{\frac{n(n-1)}{2}} \Gamma(L) \ldots \Gamma(L-n+1)$. The accuracy of the Wishart distribution to model multilook polarimetric images has been verified in previous studies [13], [14]. Functional (5) now depends on two groups of variables: The segmentation curves and the distribution parameters, i.e., the covariance matrices of the segmentation regions. The minimization of such a functional is usually done by an iterative two-step algorithm [9]:

1. fixing the curves $\{\vec{\gamma}_k\}_{k=1}^{N-1}$, i.e., the partition, and minimizing $\mathbf{E}$ with respect to the covariance matrices and
2. fixing the covariance matrices, and minimizing $\mathbf{E}$ with respect to the curves.

Minimizing $\mathbf{E}$ with respect to $\{\Sigma_{\mathbf{R}_k}\}_{k=1}^N$ is equivalent to finding the corresponding maximum-likelihood estimates $\{\hat{\Sigma}_{\mathbf{R}_k}\}_{k=1}^N$. The maximum-likelihood estimate $\hat{\Sigma}_{\mathbf{R}}$ is the empirical covariance matrix [12]

$$
\frac{\int_{\mathbf{x} \in \mathbf{R}} D(\mathbf{x}) d\mathbf{x}}{\int_{\mathbf{x} \in \mathbf{R}} d\mathbf{x}},
$$

i.e.,

$$
\hat{\Sigma}_{\mathbf{R}}(i,j) = \frac{\int_{\mathbf{x} \in \mathbf{R}} D(\mathbf{x})(i,j) d\mathbf{x}}{\int_{\mathbf{x} \in \mathbf{R}} d\mathbf{x}} \forall i \in [1..n], \forall j \in [1..n].
\tag{8}
$$

Therefore, the algorithm consists of updating $\{\hat{\Sigma}_{\mathbf{R}_k}\}_{k=1}^N$ using the empirical covariance matrices and minimizing with respect to the curves the maximum-likelihood approximation of $\mathbf{E}$, i.e.,

$$
\hat{\mathbf{E}} = \mathbf{E}|_{\{\Sigma_{\mathbf{R}_k}\}_{k=1}^N = \{\hat{\Sigma}_{\mathbf{R}_k}\}_{k=1}^N}.
$$

Using $\{\hat{\Sigma}_{\mathbf{R}_k}\}_{k=1}^N$ in the likelihood term $\mathcal{L}$ and after some algebraic manipulations, yields:

$$
\begin{aligned}
\hat{\mathcal{L}} = &A.(L.n + \log K(l,n)) + (L-n). \int_{\mathbf{x} \in \Omega} \log(\det D(\mathbf{x})) d\mathbf{x} \\
&+ L \sum_{k=1}^N a_{\mathbf{R}_k} \log(\det \hat{\Sigma}_{\mathbf{R}_k}),
\end{aligned}
\tag{9}
$$

where A is the area of the image domain and $a_{\mathbf{R}}$ is the area of a region $\mathbf{R}$. The expression $A.(L.n + \log K(l,n)) + (L-n). \int_{\mathbf{x} \in \Omega} \log(\det D(\mathbf{x})) d\mathbf{x}$ is independent of the partition and can be discarded. Therefore, the problem becomes to minimize the following functional with respect to the curves:

$$
\mathcal{F} = \sum_{k=1}^N a_{\mathbf{R}_k} \log(\det \hat{\Sigma}_{\mathbf{R}_k}) + \lambda \sum_{k=1}^{N-1} \oint_{\vec{\gamma}_k} ds.
\tag{10}
$$

2.3 The Complex Gaussian Observation Model

In the case of mono-look polarimetric images [16], [12], the image consists, at each pixel, of a complex vector $D(\mathbf{x})$ of dimension 3. In each region $\mathbf{R}$, $D(\mathbf{x})$ is assumed to follow a zero-mean circular complex Gaussian distribution [16], [12]:

$$P(D(\mathbf{x})|\mathbf{R}) = \frac{1}{\pi^n \det \Sigma_{\mathbf{R}}} \exp\left[-D(\mathbf{x})^\dagger \Sigma_{\mathbf{R}}^{-1} D(\mathbf{x})\right], \quad (11)$$

where $\dagger$ denotes the Hermitian conjugate. A classical but nontrivial calculus [18] demonstrates that the maximum-likelihood estimate of $\Sigma_{\mathbf{R}}$ in the case of the complex Gaussian distribution is given by the empirical covariance matrix

$$\hat{\Sigma}_{\mathbf{R}} = \frac{\int_{\mathbf{x}\in\mathbf{R}} D(\mathbf{x})D(\mathbf{x})^\dagger}{\int_{\mathbf{x}\in\mathbf{R}} d\mathbf{x}}.$$

Using the same computation as for the Wishart distribution, we can show that the problem of segmenting mono-look polarimetric images is equivalent to minimizing the functional defined in (10), with $\hat{\Sigma}_{\mathbf{R}_k}$ given its new meaning.

2.4 Curve Evolution Equations

To solve the problem of minimizing $\mathcal{F}$ by curve evolution in the case of two regions, we consider a simple closed parametric curve $\vec{\gamma}(s) : [0,1] \to \Omega$. We define $\mathbf{R}_1 = \mathbf{R}_{\vec{\gamma}}$ and $\mathbf{R}_2 = \mathbf{R}_1^c$. The descent equation corresponding to $\mathcal{F}$ is obtained by embedding the curve $\vec{\gamma}$ into a family of one-parameter curves $\vec{\gamma}(s,t) : [0,1] \times \Re^+ \to \Omega$ and solving the partial differential equation:

$$\frac{d\vec{\gamma}}{dt} = -\frac{\partial \mathcal{F}}{\partial \vec{\gamma}} = -\frac{\partial a_{\mathbf{R}_1} \log(\det \hat{\Sigma}_{\mathbf{R}_1}) + a_{\mathbf{R}_2} \log(\det \hat{\Sigma}_{\mathbf{R}_2})}{\partial \vec{\gamma}} - \frac{\partial \mathcal{P}}{\partial \vec{\gamma}}. \quad (12)$$

The segmentation is defined by the partition $\{\mathbf{R}_1, \mathbf{R}_2\}$ at convergence, i.e., when $t \to \infty$. The computation of $\frac{\partial \mathcal{P}}{\partial \vec{\gamma}}$ is classical and follows the standard calculus of Euler-Lagrange equations [9]:

$$\frac{\partial \mathcal{P}}{\partial \vec{\gamma}} = \frac{\partial \lambda \oint_{\vec{\gamma}} ds}{\partial \vec{\gamma}} = \lambda \kappa \vec{n}, \quad (13)$$

where κ is the mean curvature function of $\vec{\gamma}$ and $\vec{n}$ its outward unit normal. To derive the data term $\mathcal{D} = a_{\mathbf{R}_1} \log(\det \hat{\Sigma}_{\mathbf{R}_1}) + a_{\mathbf{R}_2} \log(\det \hat{\Sigma}_{\mathbf{R}_2})$ with respect to $\vec{\gamma}$, we propose a computation based on its first order expansion rather than the Euler-Lagrange equation. This has the advantage of leading to a clear interpretation of how to embed a simple, efficient partition constraint directly in multiphase curve evolution. Let $\vec{\delta\gamma} = (\delta x, \delta y)^T = \delta\gamma.\vec{n}$ be an elementary local deformation of $\vec{\gamma}$ ($\|\vec{\delta\gamma}\| = 1$) around a pixel $s = (x,y)$, where $\vec{n}$ is the external unit normal to $\vec{\gamma}$ at $s = (x,y)$. We have:

$$\mathcal{D}(\vec{\gamma} + \vec{\delta\gamma}) = \mathcal{D}(x + \delta x, y + \delta y)$$
$$= \mathcal{D}(x,y) + \frac{\partial \mathcal{D}}{\partial x}\delta x + \frac{\partial \mathcal{D}}{\partial y}\delta y \quad (14)$$
$$= \mathcal{D}(\vec{\gamma}) + \frac{\partial \mathcal{D}}{\partial \vec{\gamma}}.\vec{\delta\gamma}.$$

This implies:

$$\frac{\partial \mathcal{D}}{\partial \vec{\gamma}}.\|\vec{\delta\gamma}\| = \frac{\partial \mathcal{D}}{\partial \vec{\gamma}} = \left(\mathcal{D}(\vec{\gamma} + \vec{\delta\gamma}) - \mathcal{D}(\vec{\gamma})\right).\vec{\delta\gamma}. \quad (15)$$

Consider the local variation $\Delta\mathcal{D}(s) = \mathcal{D}(\vec{\gamma} + \vec{\delta\gamma}) - \mathcal{D}(\vec{\gamma})$. We have: $\Delta\mathcal{D}(s) = \Delta_{\mathbf{R}_1}(s) + \Delta_{\mathbf{R}_2}(s)$, where:

$$\Delta_{\mathbf{R}}(s) = (a_{\mathbf{R}} + \delta a_{\mathbf{R}}) \log(\det \hat{\Sigma}_{\mathbf{R}} + \delta \det \hat{\Sigma}_{\mathbf{R}})$$
$$- a_{\mathbf{R}} \log(\det \hat{\Sigma}_{\mathbf{R}}), \mathbf{R} = (\mathbf{R}_1, \mathbf{R}_2). \quad (16)$$

$\delta a_{\mathbf{R}}$ is the elementary variation of the area of $\mathbf{R}$. $\delta a_{\mathbf{R}} = 1$ if the curve is locally expanding around a pixel $s = (x,y)$ to contain it and $\delta a_{\mathbf{R}} = -1$ when the curve is shrinking. $\delta \det \hat{\Sigma}_{\mathbf{R}}$ is the elementary variation of $\det \hat{\Sigma}_{\mathbf{R}}$. We also have:

$$\log(\det \hat{\Sigma}_{\mathbf{R}} + \delta \det \hat{\Sigma}_{\mathbf{R}}) = \log(\det \hat{\Sigma}_{\mathbf{R}})$$
$$+ \frac{\partial \log(\det \hat{\Sigma}_{\mathbf{R}})}{\partial \det \hat{\Sigma}_{\mathbf{R}}}.\delta \det \hat{\Sigma}_{\mathbf{R}}. \quad (17)$$

To compute the elementary variation $\delta \det \hat{\Sigma}_{\mathbf{R}}$, we need to compute the variation $\delta\hat{\Sigma}_{\mathbf{R}}(i,j), \forall i, j$. We describe a computation for the multilook case, but the same method applies to the mono-look case. Let $S_{\mathbf{R}}(i,j) = \int_{\mathbf{x}\in\mathbf{R}} D(\mathbf{x})(i,j)d\mathbf{x}$. We have:

$$\delta\hat{\Sigma}_{\mathbf{R}}(i,j) = \frac{S_{\mathbf{R}}(i,j) + \delta a_{\mathbf{R}} D(s)(i,j)}{a_{\mathbf{R}} + \delta a_{\mathbf{R}}} - \frac{S_{\mathbf{R}}(i,j)}{a_{\mathbf{R}}}$$
$$= \frac{\delta a_{\mathbf{R}}}{a_{\mathbf{R}} + \delta a_{\mathbf{R}}}\left(D(s)(i,j) - \hat{\Sigma}_{\mathbf{R}}(i,j)\right). \quad (18)$$

Then, the first order expansion of $\det \hat{\Sigma}_{\mathbf{R}}$ is, after algebraic manipulations and where $n = 3$ is the data matrix dimension:

$$\delta \det \hat{\Sigma}_{\mathbf{R}} = \sum_{i,j} \frac{\partial \det \hat{\Sigma}_{\mathbf{R}}}{\partial \hat{\Sigma}_{\mathbf{R}}(i,j)} \delta\hat{\Sigma}_{\mathbf{R}}(i,j)$$
$$= \frac{\delta a_{\mathbf{R}}}{a_{\mathbf{R}} + \delta a_{\mathbf{R}}} \det \hat{\Sigma}_{\mathbf{R}}\left(tr(\hat{\Sigma}_{\mathbf{R}}^{-1} D(s)) - n\right). \quad (19)$$

Combining (16), (17), and (18), we have, after some algebraic manipulations:

$$\Delta_{\mathbf{R}}(s) = \delta a_{\mathbf{R}}\left(\log(\det \hat{\Sigma}_{\mathbf{R}}) + tr(\hat{\Sigma}_{\mathbf{R}}^{-1} D(s)) - n\right). \quad (20)$$

Suppose, without loss of generality, that $\vec{\gamma}$ is expanding to contain s, i.e., $\delta a_{\mathbf{R}_1} = 1$ and $\delta a_{\mathbf{R}_2} = -\delta a_{\mathbf{R}_1} = -1$ because $\mathbf{R}_2 = \mathbf{R}_1^c$, then,

$$\Delta_{\mathbf{R}_1}(s) = \Delta_{\mathbf{R}_1}^+(s) = \left(\log(\det \hat{\Sigma}_{\mathbf{R}_1}) + tr(\hat{\Sigma}_{\mathbf{R}_1}^{-1} D(s)) - n\right),$$
$$\Delta_{\mathbf{R}_2}(s) = -\Delta_{\mathbf{R}_2}^+(s) = -\left(\log(\det \hat{\Sigma}_{\mathbf{R}_2}) + tr(\hat{\Sigma}_{\mathbf{R}_2}^{-1} D(s)) - n\right). \quad (21)$$

$\Delta_{\mathbf{R}}^+(s)$ is the variation of the data term $\mathcal{D}$ corresponding to the variation of $a_{\mathbf{R}} \log(\det \hat{\Sigma}_{\mathbf{R}})$ when a pixel s enters the region $\mathbf{R}$. Using (15) and (20) yields:

$$\frac{\partial \mathcal{D}}{\partial \vec{\gamma}} = \left(\Delta_{\mathbf{R}_1}^+(s) - \Delta_{\mathbf{R}_2}^+(s)\right).\vec{\delta\gamma} = \left(\log(\det \hat{\Sigma}_{\mathbf{R}_1}) + tr(\hat{\Sigma}_{\mathbf{R}_1}^{-1} D(s))\right.$$
$$\left. - \log(\det \hat{\Sigma}_{\mathbf{R}_2}) - tr(\hat{\Sigma}_{\mathbf{R}_2}^{-1} D(s))\right).\vec{\delta\gamma}. \quad (22)$$

When $\vec{\gamma}$ is expanding, we also have: $\vec{\delta\gamma} = \vec{n}$. Therefore, the functional derivative of $\mathcal{D}$ with respect to $\vec{\gamma}$ is:

$$\frac{\partial \mathcal{D}}{\partial \vec{\gamma}} = \left(\Delta_{\mathbf{R}_1}^+(s) - \Delta_{\mathbf{R}_2}^+(s)\right).\vec{n}. \quad (23)$$

When $\vec{\gamma}$ is shrinking at s leads to the same expression. Adding (13) to (23), and using (12) give the final evolution equation for $\vec{\gamma}$:

$$\frac{d\vec{\gamma}}{dt} = -\frac{\partial \mathcal{F}}{\partial \vec{\gamma}} = -\left(\Delta_{\mathbf{R}_1}^+(s) - \Delta_{\mathbf{R}_2}^+(s) + \lambda\kappa\right)\vec{n}. \qquad (24)$$

2.5 Level Set Implementation

We use the level set representation [19] to implement the evolution equation (24). With the level set representation, curve $\vec{\gamma}$ is represented implicitly as the zero level set of a function $u : \mathbb{R}^2 \to \mathbb{R}$, i.e., $\vec{\gamma}$ is the set $\{u = 0\}$. The level set evolution equation corresponding to (24) is [19]:

$$\frac{\partial u}{\partial t}(\mathbf{x}, t) = -\left(\Delta_{\mathbf{R}_1}^+(\mathbf{x}) - \Delta_{\mathbf{R}_2}^+(\mathbf{x}) + \lambda\kappa_{u_1}\right)\|\vec{\nabla}u(\mathbf{x}, t)\|, \quad (25)$$

where $\Delta_{\mathbf{R}}^+(\mathbf{x}) = \log(\det\Sigma_{\mathbf{R}}) + tr(\Sigma_{\mathbf{R}}^{-1}D(\mathbf{x})) - n, \forall \mathbf{x} \in \mathbf{R}$. κ_u is the curvature of $\{u = 0\}$.

2.6 Extension to Multiphase Segmentation

Consider a family of simple closed curves $\vec{\gamma}_k|_{k=1,\dots,N-1}$ and let $\mathbf{R}_k = \mathbf{R}_{\vec{\gamma}_k}|_{k=1,\dots,N-1}$. Let $\mathbf{R}_N = \bigcap_{i=1}^{N-1}\mathbf{R}_i^c$. We will impose a simple, efficient partition constraint directly on the multiphase curve evolution as follows:

Partition Constraints.

1. Start from an initial partition $\mathbf{P}^0 = \{\mathbf{R}_k^0\}_{k\in[1,N]}$.
2. Suppose we have a partition $\mathbf{P}^t = \{\mathbf{R}_k^t\}_{k\in[1,N]}$ at iteration t, and let $\mathbf{x} \in \Omega$. If $\mathbf{x} \in \mathbf{R}_i^t, i \in [1,..,N]$ and $\mathbf{x}$ leaves region $\mathbf{R}_i^t$, it must move to another region $\mathbf{R}_j, j \in [1..N], j \neq i$, and only one other region, i.e., $\mathbf{x} \in \mathbf{R}_j^{t+1}$ and $\forall k \neq j, \mathbf{x} \notin \mathbf{R}_k^{t+1}$.

To satisfy Condition 2, the curve evolution equations at pixel $\mathbf{x}$ must involve at most two curves, i.e., only two regions: region $\mathbf{R}_i$ which contains pixel $\mathbf{x}$ and another region $\mathbf{R}_j, j \neq i$. To obtain the multiphase curve evolution equations satisfying Condition 2, we fix curves $\vec{\gamma}_k, k \notin \{i, j\}$, and minimize the functional with respect to the variation of $\vec{\gamma}_i$ if $i \neq N$, and $\vec{\gamma}_j$ if $j \neq N$, i.e.,

$$\text{if } i \neq N, \frac{\partial \mathcal{F}}{\partial \vec{\gamma}_i}$$
$$= \frac{\partial\left(a_{\mathbf{R}_i}\log\det(\hat{\Sigma}_{\mathbf{R}_i}) + a_{\mathbf{R}_j}\log\det(\hat{\Sigma}_{\mathbf{R}_j})\right)}{\partial\vec{\gamma}_i} + \frac{\partial\lambda\oint_{\vec{\gamma}_i}ds}{\partial\vec{\gamma}_i},$$
$$\text{if } j \neq N, \frac{\partial \mathcal{F}}{\partial \vec{\gamma}_j} \qquad\qquad (26)$$
$$= \frac{\partial\left(a_{\mathbf{R}_i}\log\det(\hat{\Sigma}_{\mathbf{R}_i}) + a_{\mathbf{R}_j}\log\det(\hat{\Sigma}_{\mathbf{R}_j})\right)}{\partial\vec{\gamma}_j} + \frac{\partial\lambda\oint_{\vec{\gamma}_j}ds}{\partial\vec{\gamma}_j}.$$

Therefore, multiregion segmentation reduces to a two-region problem corresponding to the variation $\Delta_{\mathbf{R}_i} + \Delta_{\mathbf{R}_j}$ of $\mathcal{D}$ in the domain $\mathbf{R}_i \cup \mathbf{R}_j$. Following the computation in the two-region case, the level-set curve evolution equations corresponding to the minimization of $\mathcal{F}$ with respect to $\vec{\gamma}_i$, if $i \neq N$, and with respect to $\vec{\gamma}_j$, if $j \neq N$ are given by:

$$\text{if } i \neq N, \frac{\partial u_i}{\partial t}(\mathbf{x}, t) = -\left(\Delta_{\mathbf{R}_i}^+(\mathbf{x}) - \Delta_{\mathbf{R}_j}^+(\mathbf{x}) + \lambda\kappa_{u_i}\right)\|\vec{\nabla}u_i(\mathbf{x}, t)\|,$$
$$\text{if } j \neq N, \frac{\partial u_j}{\partial t}(\mathbf{x}, t) = -\left(\Delta_{\mathbf{R}_j}^+(\mathbf{x}) - \Delta_{\mathbf{R}_i}^+(\mathbf{x}) + \lambda\kappa_{u_j}\right)\|\vec{\nabla}u_j(\mathbf{x}, t)\|,$$
$$(27)$$

where u_k is the level-set function corresponding to $\vec{\gamma}_k, k \in [1..N-1]$, and κ_{u_k}, is the curvature of the zero level-set of u_k. It is clear that the curve evolution equations defined in system (27) satisfy the partition condition 2. If $i = N$ or $j = N$, the system (27) is equivalent to only one evolution equation corresponding to the two-region segmentation problem in the domain $\mathbf{R}_i \cup \mathbf{R}_j$. If $i \neq N$ and $j \neq N$ and if we ignore the contribution of the curvature term, the two evolving curves $\vec{\gamma}_i$ and $\vec{\gamma}_j$ have opposite velocities at point $\mathbf{x}$. Thus, if $\vec{\gamma}_i$ shrinks at $\mathbf{x}$, $\vec{\gamma}_j$ expands to contain it and vice versa. If the contribution of the curvature term is important, both evolving curves shrink and $\mathbf{x}$ leaves the interior of one curve to enter the background region $\mathbf{R}_N$. The problem now is the definition of the region $\mathbf{R}_j, j \in [1..N], j \neq i$, that will be involved in system (27) at a given pixel $\mathbf{x} \in \Omega$. Let $\mathbf{x} \in \mathbf{R}_i$ and suppose $\mathbf{x}$ leave $\mathbf{R}_i$ to enter $\mathbf{R}_j, j \in [1..N], j \neq i$. The resulting variation of the data term $\mathcal{D}$ is $\Delta_{\mathbf{R}_j}^+(\mathbf{x}) - \Delta_{\mathbf{R}_i}^+(\mathbf{x})$. Since we aim to minimize $\mathcal{F}$, the best variation is given by:

$$j_0 = \arg \min_{\{j\in[1..N], \mathbf{x}\notin\mathbf{R}_j\}}\left(\Delta_{\mathbf{R}_j}^+(\mathbf{x}) - \Delta_{\mathbf{R}_i}^+(\mathbf{x})\right)$$
$$= \arg \min_{\{j\in[1..N], \mathbf{x}\notin\mathbf{R}_j\}}\Delta_{\mathbf{R}_j}^+(\mathbf{x}). \qquad (28)$$

This leads to the following multiphase level set equations, for all $\mathbf{x} \in \Omega$:

$$\forall i \in [1..N], if \ \mathbf{x} \in \mathbf{R}_i, \ do$$
$$1) \text{ if } i \neq N, \frac{\partial u_i}{\partial t}(\mathbf{x}, t)$$
$$= -\left(\Delta_{\mathbf{R}_i}^+(\mathbf{x}) - \Delta_{\mathbf{R}_{j_0}}^+(\mathbf{x}) + \lambda\kappa_{u_i}\right)\|\vec{\nabla}u_i(\mathbf{x}, t)\|, \qquad (29)$$
$$2) \text{ if } j_0 \neq N, \frac{\partial u_{j_0}}{\partial t}(\mathbf{x}, t)$$
$$= -\left(\Delta_{\mathbf{R}_{j_0}}^+(\mathbf{x}) - \Delta_{\mathbf{R}_i}^+(\mathbf{x}) + \lambda\kappa_{u_{j_0}}\right)\|\vec{\nabla}u_{j_0}(\mathbf{x}, t)\|,$$

where $i \in [1..N]$ is the index of the region containing $\mathbf{x}$ and j_0 is given by (28).

As with other multiphase methods, this method converges to a local minimum. However, it is stepwise optimal because it effects the maximum decrease in the functional at each curve evolution step. This comes directly from the definition of j_0 in (28).

This multiphase method has a computational advantage over the methods in [3], [5], [17], [1]. It activates at most two level sets at each iteration. The CPU time varies approximately linearly with the number of regions due to the search for index j_0. The methods in [3],[5], [17], [1] activate all the level sets at each iteration and the complexity of the corresponding PDEs increases with the number of regions. The methods in [3], [5] also evaluate an expensive point membership function. For the method in [5], this involves, for a given level set, checking the sign of all lower numbered level sets. For the method in [3], this involves
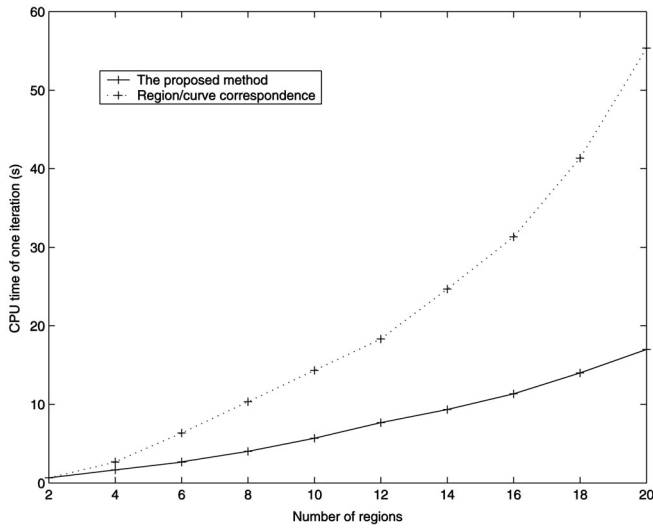
Fig. 1. CPU time versus the number of regions.

Fig. 2. Region distributions in the image D(.)(1,1) corresponding to the synthetic circle data.

checking the signs of all level set intersections. This results in a variation of the computation time versus the number of regions faster than linear. Fig. 1 illustrates this. It shows the CPU time spent at an iteration as a function of the number of regions for this method and the method in [5]. The growth of the curve for the method in [3] would be similar to the one for the method in [5] or steeper.

3 EXPERIMENTATION

The proposed algorithm has been tested on a wide range of real, fully polarimetric NASA-JPL images and on three synthetic images to evaluate quantitatively and comparatively the method. In the following, we present few representative results.
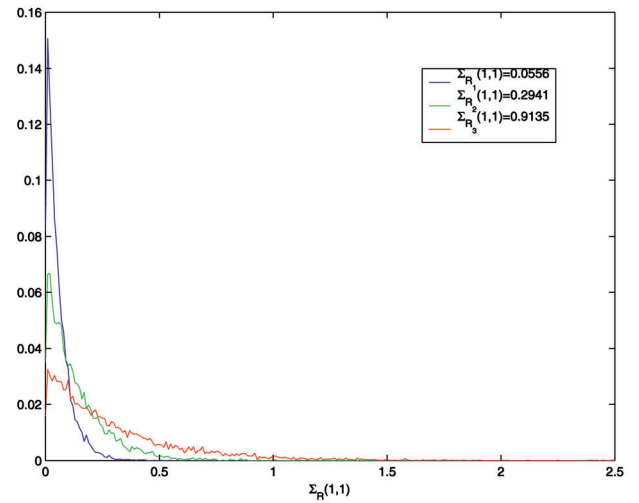
Simulated data: The first synthetic image is generated using the ideal segmentation image in Fig. 3a and the complex Gaussian distribution. The region parameters are taken from homogeneous regions in a real image. To display the image, we use only the first coefficient of the pixel matrix D(x), i.e., the real image $D(\mathbf{x})(1,1)$. For viewing purposes only, we enhanced the contrast (Fig. 3b). Otherwise, the gray-level value in regions would be overlapped as displayed in Fig. 3c. An illustration of the overlap between the distribution of regions in $D(\mathbf{x})(1,1)$ is given in Fig. 2. The same display method is used for the other results, and the displayed images are just modified gray-level representations of the full complex data. Thus, the visual interpretation of the results is insufficient and quantitative evaluation using ideal segmentation image as a reference is required. We show the
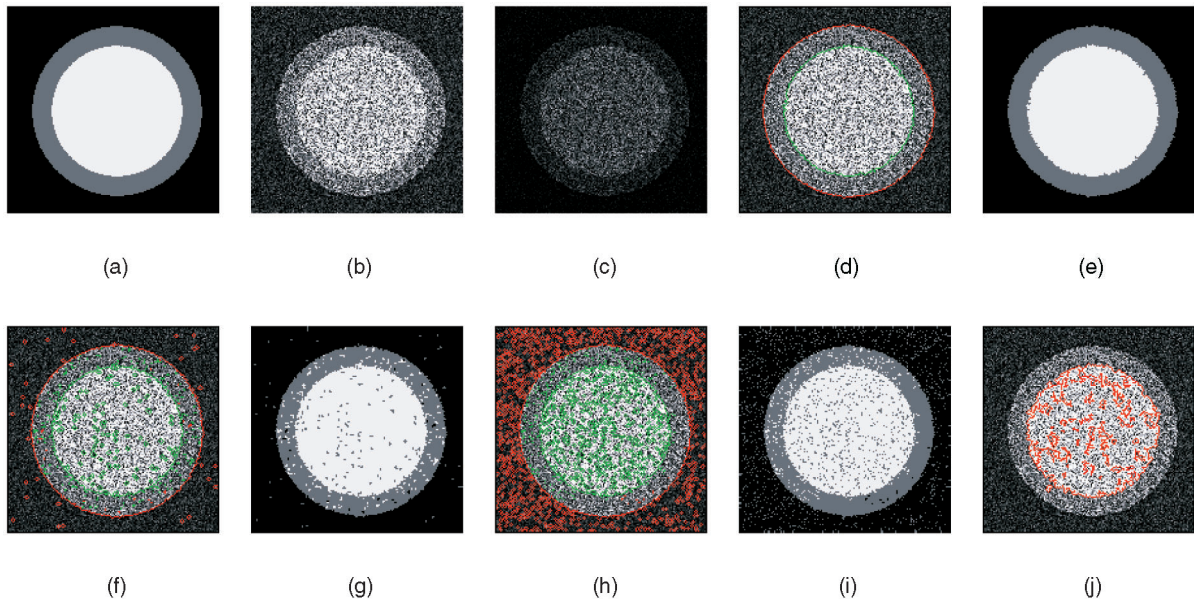

(a)　　　　(b)　　　　(c)　　　　(d)　　　　(e)

(f)　　　　(g)　　　　(h)　　　　(i)　　　　(j)

Fig. 3. Results of the synthetic circle data: (a) ideal segmentation, (b) display of D(.)(1,1) with histogram modification, (c) display of D(.)(1,1) without histogram modification, (d) and (e) results with $\lambda = 0.2$, (f) and (g) results with $\lambda = 0.001$, (h) and (i) results with $\lambda = 0$, and (j) result using the Gaussian model and D(.)(1,1).

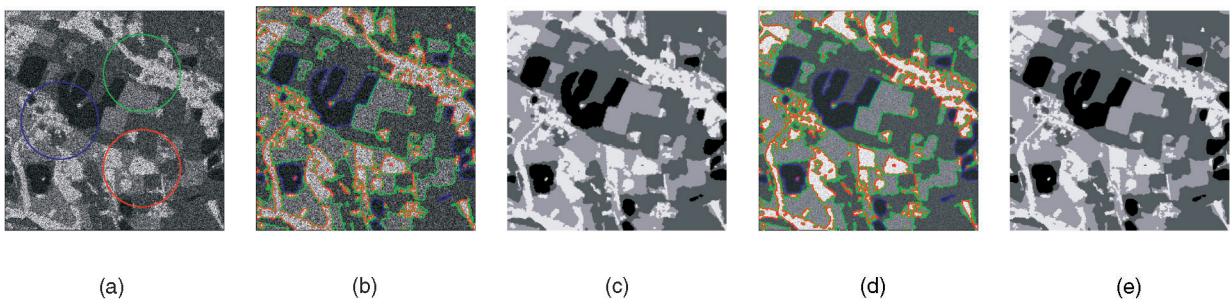(a)   (b)   (c)   (d)   (e)

Fig. 4. Results of the 1-look synthetic data: (a) initial curves, (b) final position of the curves, and (c) segmentation result. Results of the eight-look synthetic data: (d) final position of the curves and (e) segmentation result.

TABLE 1
Comparisons

Contour-based comparison	8-look	1-look	Region-based comparison	8-look	1-look
LACLM	96.49%	77.00%	LACLM	99.14%	94.84%
RMLM	94.40%	69.75%	RMLM+SBC	98.72%	92.31%

final position of curves in Fig. 3d and the segmentation result in Fig. 3e for $\lambda = 0.2$ (each curve is represented by a color). To show the effect of the regularization parameter λ, we display the results with $\lambda = 0.001$ and $\lambda = 0$ in Figs. 3f, 3g, 3h, and 3i. We obtain many small islands in the result with a smaller weight of the regularization term. To illustrate the influence of the observation model, we show in Fig. 3j the result obtained by applying the Gaussian model to $D(.)(1,1)$. The green curve disappeared and the red curve gave erroneous results.

To simulate realistic situations, we take a segmentation result of a real polarimetric image as the ideal segmentation to generate two 512×512 images of four regions. The first is mono-look, generated from the complex Gaussian distribution, and the second is 8-look, generated from the complex Wishart distribution. Fig. 4a show initial curves for the two simulated images. Fig. 4b and Fig. 4d show, respectively, the final position of the curves for the 1-look image and the 8-look image. Figs. 4c and 4e display the segmentation results.

Comparative Evaluation: We compared the performance of the proposed method, which we refer to as LACLM (Level Set Active Contour Likelihood Maximization) to the recent segmentation method developed in [12] and based on hierarchical region merging, which we refer to as RMLM (Region Merging Likelihood Maximization). We chose this method for comparison because it optimizes a global like-lihood criterion, as with the proposed method. We notice that the merging of neighboring regions in RMLM cannot classify directly the image into regions with disjoint segments as our method did. To obtain a classification into four classes, we need to classify the connected segments given by RMLM. To compare directly RMLM and LACLM, we used contour information in the segmentation result of each method (i.e., pixels where the image gradient in the segmentation result is not equal to zero). We compare with the RMLM segmentation into 250 segments. As expected, the LACLM gives more regular boundaries than RMLM, especially for the one-look

image. Moreover, as shown in Table 1, and although the level of details is more important with RMLM than with LACLM, the percentage of correctly detected contour pixels is better with LACLM. To examine more carefully the performance of the proposed method, we added a supervised Bayesian classification (SBC) to the segmentation results of RMLM, i.e., we used the region parameters to classify the 250 connected segments produced by RMLM into four classes. This is not a point of relevance in practice because the region parameters are unknown in real situations. We notice, in our method, that the region parameters are estimated iteratively along the segmentation process in an unsupervised way. Although the method based on RMLM and SBC is supervised, the proportion of correctly classified pixels with LACLM is, as shown in Table 1, better.

We show results on two multilook fully polarimetric NASA-JPL images. The first image, represented in Fig. 5a (with final curves) is an extract of 512×800 pixels from the NASA-JPL image of Flevoland (Netherland). The second image, represented in Fig. 5c (with final curves) is an extract of 512×800 pixels from the NASA-JPL image of Altona (Canada). We segmented the two images into six regions. Figs. 5b and 5d display the segmentation results. The visual display of the results illustrates the performances of the method. To evaluate the robustness of the method with respect to initial conditions, we tested the four different initialization represented in Figs. 6a, 6b, 6c, and 6d, and plotted the minimized energies versus iterations in Fig. 7. All the minimized energies converge to the same minimum. This demonstrates the robustness of the method to initialization.

4   CONCLUSION

We presented a level set curve evolution algorithm for segmenting polarimetric images into a fixed but arbitrary number of complex Wishart/Gaussian distributed regions. We defined an efficient multiphase system of multiple curve
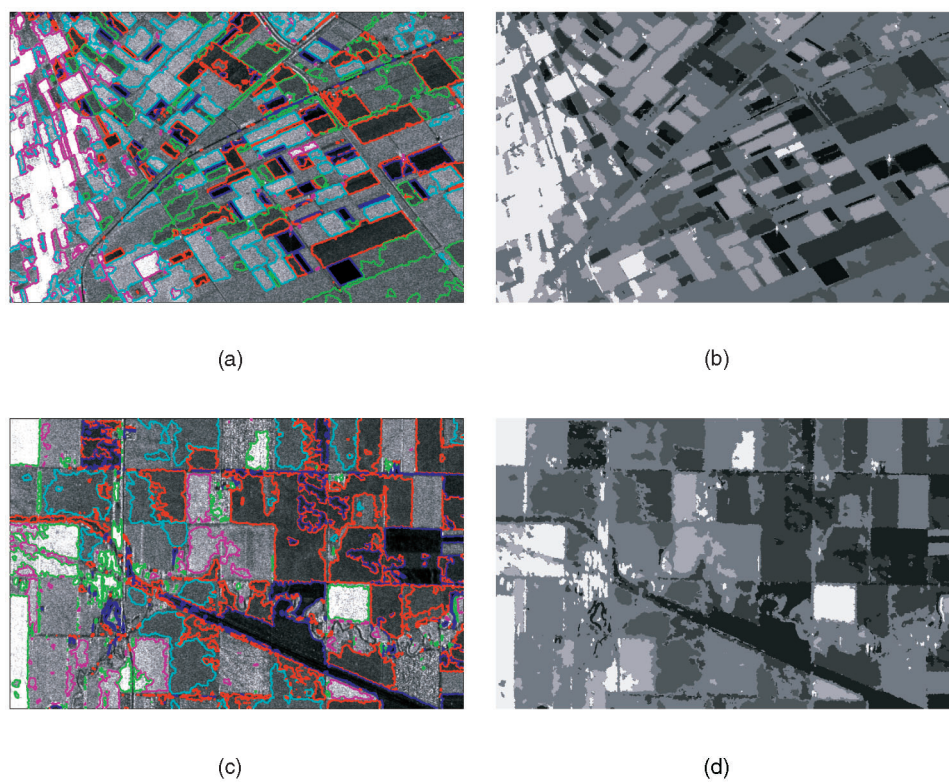
(a)

(b)

(c)

(d)

Fig. 5. Results for the real images: (a) final position of the curves for the Flevoland data, (b) segmentation result for the Flevoland data, (c) final position of the curves for the Altona data, and (d) segmentation result for the Altona data.
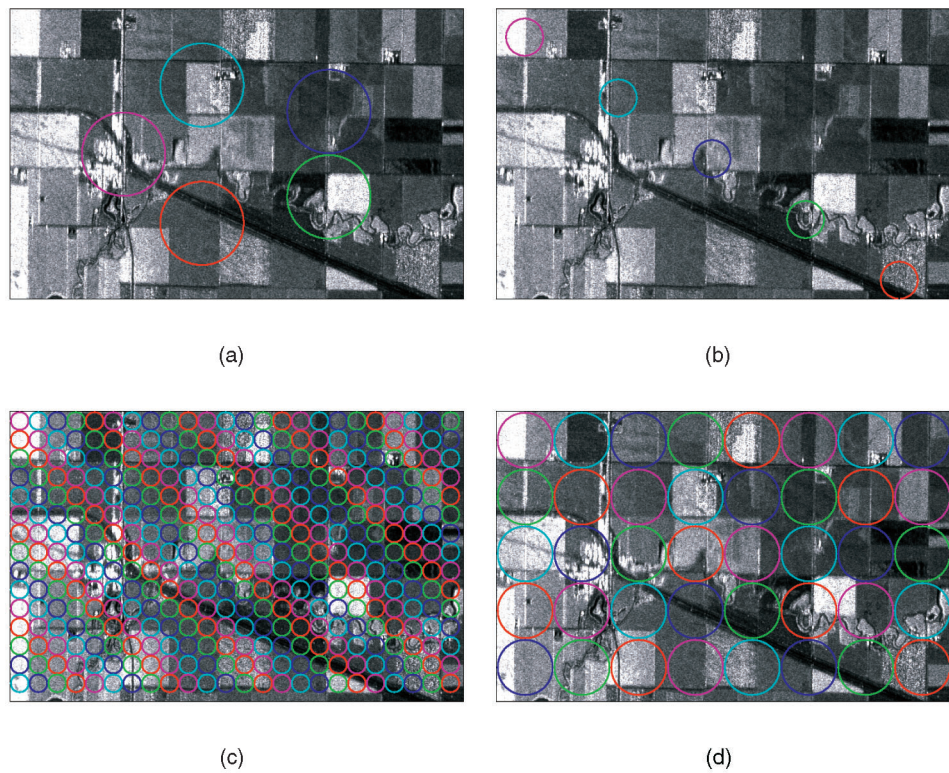

(a)

(b)

(c)

(d)

Fig. 6. Four different initializations.

evolution equations which minimize the sum of an original data term derived from the maximum-likelihood approximation and a prior term related to the length of the curves. The algorithm was illustrated on both simulated and real polarimetric images. We provided quantitative evaluation of the method as well as comparisons with another recent method. The method is also shown to be robust to initial partition.
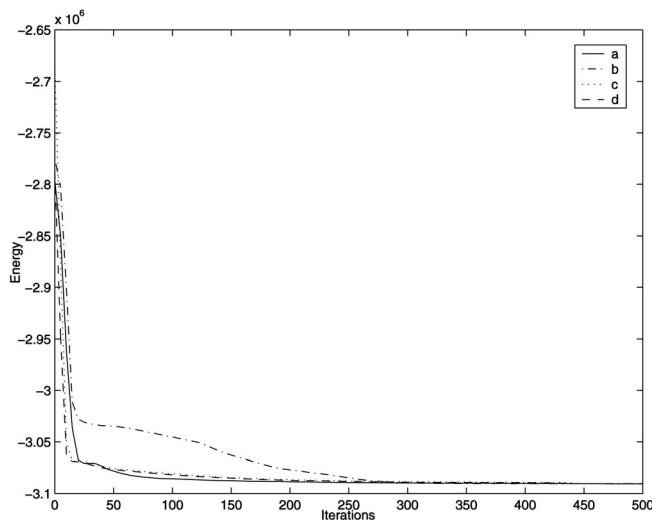
Fig. 7. Energy versus iterations for different initializations.

ACKNOWLEDGMENTS

REFERENCES

[1]   C. Samson, L. Blanc-Féraud, G. Aubert, and J. Zerubia, "A Level Set Model for Image Classification," *Int'l J. Computer Vision,* vol. 40, no. 3, pp. 187-197, Mar. 2000.

[2]   T. Chan and L. Vese, "Active Contours without Edges," *IEEE Trans. Image Processing,* vol. 10, no. 2, pp. 266-277, 2001.

[3]   L. Vese and T. Chan, "A Multiphase Level Set Framework for Image Segmentation Using the Mumford and Shah Model," *Int'l J. Computer Vision,* vol. 50, no. 3, pp. 271-293, 2002.

[4]   A. Yezzi, A. Tsai, and A. Willsky, "A Fully Global Approach to Image Segmentation via Coupled Curve Evolution Equations," *J. Visual Comm. and Image Representation,* vol. 13, no. 1, pp. 195-216, Mar. 2002.

[5]   A.-R. Mansouri, A. Mitiche, and C. Vazquez, "Multiregion Competition: A Level Set Extension of Region Competition to Multiple Region Image Partitioning," *Computer Vision and Image Understanding,* vol. 101, no. 3, pp. 137-150, Mar. 2006.

[6]   N. Paragios, O. Mellina-Gottardo, and V. Ramesh, "Gradient Vector Flow Fast Geometric Active Contours," *IEEE Trans. Pattern Analysis and Machine Intelligence,* vol. 26, no. 3, pp. 402-407, Mar. 2004.

[7]   I. Ben Ayed, A. Mitiche, and Z. Belhadj, "Multiregion Level Set Partitioning of Synthetic Aperture Radar Images," *IEEE Trans. Pattern Analysis and Machine Intelligence,* vol 27, no. 5, pp. 793-800, May 2005.

[8]   D. Mumford and J. Shah, "Optimal Approximation by Piecewise Smooth Functions and Associated Variational Problems," *Comm. Pure Applied Math.,* vol. 42, pp. 577-685, 1989.

[9]   S.C. Zhu and A. Yuille, "Region Competition: Unifying Snakes, Region Growing, and Bayes/MDL for Multiband Image Segmentation," *IEEE Trans. Pattern Analysis and Machine Intelligence,* vol. 18, no. 9, pp. 884-900, Sept. 1996.

[10]   P. Martin, P. Réfrégier, F. Goudail, and F. Guérault, "Influence of the Noise Model on Level Set Active Contour Segmentation," *IEEE Trans. Pattern Analysis and Machine Intelligence,* vol. 26, no. 6, pp 799-803, June 2004.

[11]   S.L. Jacques, J.C. Ramella-Roman, and K. Lee, "Imaging Skin Pathology with Polarized Light," *J. Biomedical Optics,* vol. 7, pp. 329-340, 2002.

[12]   J.M. Beaulieu and R. Touzi, "Segmentation of Textured Polarimetric SAR Scenes by Likelihood Approximation," *IEEE Trans. Geoscience and Remote Sensing,* vol. 42, pp. 2063-2072, 2004.

[13]   K. Conradsen, A.A. Nielsen, J. Schou, and H. Skriver, "A Test Statistic in the Complex Wishart Distribution and Its Application to Change Detection in Polarimetric SAR Data," *IEEE Trans. Geoscience and Remote Sensing,* vol. 41, no. 1, pp. 4-19, 2003.

[14]   P.R. Kersten, J.-S. Lee, and T.L. Ainsworth, "Unsupervised Classification of Polarimetric Synthetic Aperture Radar Images Using Fuzzy Clustering and EM Clustering," *IEEE Trans. Geoscience and Remote Sensing,* vol. 43, no. 3, pp. 519-527, 2005.

[15]   Y. Dong, A.K. Milne, and B.C. Forester, "Segmentation and Classification of Vegetated Areas Using Polarimetric SAR Image Data," *IEEE Trans. Geoscience and Remote Sensing,* vol. 39, no. 2, pp. 321-329, 2001.

[16]   F. Goudail and P. Réfrégier, "Contrast Definition for Optical Coherent Polarimetric Images," *IEEE Trans. Pattern Analysis and Machine Intelligence,* vol. 26, pp. 947-951, 2004.

[17]   H.-k. Zhao, T. Chan, B. Merriman, and S. Osher, "A Variational Level Set Approach to Multiphase Motion," *J. Computational Physics,* vol. 127, pp. 179-195, Sept. 1996.

[18]   R.J. Muirhead, *Aspects of Multivariate Statistical Theory.* New York: Wiley, 1982.

[19]   J.A. Sethian, *Level Set Methods and Fast Marching Methods,* second ed. Cambridge Univ. Press, 1999.

Ismail Ben Ayed received the Bachelor's degree and the MS degree in telecommunications from the École Supérieure des Communications de Tunis (SUP'COM), Tunisia in 2002 and 2003, respectively. He is completing the PhD degree in the Telecommunications' Department, Institut National de la Recherche Scientifique, Montréal, Quebec, Canada. He authored more than 10 research papers in leading journals and conferences. His research interests include image and motion segmentation with a focus on variational techniques, statistical modeling and shape representation for image analysis, and remote sensing. He is a student member of the IEEE, the IEEE Computer Society, and the IEEE Signal Processing Society.

Amar Mitiche holds a Licence Ès Sciences in mathematics from the University of Algiers and the PhD degree in computer science from the University of Texas at Austin. He is currently a professor at the Institut National de Recherche Scientifique (INRS), department of telecommunications, in Montréal, Quebec, Canada. His research is in computer vision. His current interests include image segmentation, motion analysis in monocular and stereoscopic image sequences (detection, estimation, segmentation, tracking, 3D interpretation) with a focus on level set methods, and written text recognition with a focus on neural networks methods. He is a member of the IEEE.

Ziad Belhadj received the Habilitation Universitaire in Information technology and Communication degree in 2001, the PhD degree in computer systems from the Ecole Polytechnique de Nantes (Formerly IRESTE), France in 1995. After a postdoctoral at JPL, he joined the École Supérieure des Communications de Tunis (SUP'COM) in 1996 where he is now a professor, responsible of Urisa research laboratory and PhD degrees in information technology. His research interests include satellite image processing, speckle denoising from SAR images, remote sensing, image classification, 3D reconstruction, and satellite image indexation. He is a member of the IEEE.

▷ **For more information on this or any other computing topic, please visit our Digital Library at** www.computer.org/publications/dlib.